Innov Biosyst Bioeng, 2024, vol. 8, no. 3, 29–49
doi: 10.20535/ibb.2024.8.3.292667

Original article

EFFECT OF MAGNETIC FIELD AND MAGNETIC NANOPARTICLES ON CHOICE OF ENDOTHELIAL CELL PHENOTYPE

S.V. Gorobets, O.Yu. Gorobets*, K.O. Rachek, A.M. Ryazanova

Igor Sikorsky Kyiv Polytechnic Institute, Kyiv, Ukraine

*Corresponding author: gorobets.oksana@gmail.com

Received 7 December 2023; Accepted 1 July 2024

Background. Endothelial cells as participants in angiogenesis choose their phenotype as tip cells (leading, migratory) or stalk cells (following). It has been experimentally found and theoretically modeled that rapid oscillations in intracellular calcium concentration play a key role in controlling phenotype selection and possible vessel architecture. In addition, the intracellular calcium concentration in endothelial cells is known to be regulated by mechanical wall shear stress induced by blood flow, which controls mechanosensitive calcium ion channel gating. Experimental methods of controlling mechanosensitive ion channel gating in external magnetic fields with application of magnetic nanoparticles are developed that affect magnetic nanoparticles artificially attached to cell membranes.

Objective. A key question is raised about the possibility of controlled selection of endothelial cell phenotype in external magnetic fields due to the presence of artificial or biogenic magnetic nanoparticles embedded in the cell membrane.

Methods. The magnetic wall shear stress is calculated due to the influence of the external magnetic field on the magnetic nanoparticles embedded in the cell membrane, which controls the mechanosensitive calcium ion pathways. Numerical modeling of oscillations in intracellular calcium concentration in endothelial cells and determination of their final phenotype was carried out taking into account intercellular communication. The python programming language and scipy, py-pde, matplotlib packages of the python programming language were used for numerical modeling.

Results. The magnetic field flux density and frequency ranges of a uniform rotating magnetic field, as well as the magnitude of the gradient and the frequency of a non-uniform oscillating magnetic field were calculated for controlling the amplitude and frequency of intracellular calcium concentration oscillations in endothelial cells, as well as the selection of their phenotype. It opens the perspective of controlling angiogenesis and vessel architecture.

Conclusions. Phenotype selection by endothelial cells can be controlled in a uniform rotating external magnetic field, as well as in a non-homogeneous oscillating magnetic field.

Keywords: gradient magnetic field; rotating magnetic field; endothelial cells; intracellular calcium concentration; phenotype selection; magnetic nanoparticles.

Introduction

Influence of magnetic fields (MP) on composition [1], viscosity [2–4], blood dynamics [3, 5] and proliferation of the endothelium [6, 7] and, accordingly, angiogenesis remains a topic that has been limitedly researched in the scientific literature, which is characterized by considerable ambiguity in the results of research by different authors [8]. Within the existing data of experimental studies, there are conflicting results regarding the influence of magnetic fields on perfusion and blood pressure [8]. Approximately half of the studies mentioned in the review [8] suggest that magnetic fields have a vasodilator effect, while the other half of studies found that magnetic fields can cause either vasodilation or vasoconstriction depending on the initial state of vascular tone [8]. Some studies even indicate that magnetic fields can reduce perfusion or have no noticeable effect at all [8]. In most works, the stimulation of angiogenesis under the influence of magnetic fields was found [8–14], however, the opposite effect was reported in a number of works [8, 15, 16]. For example, the effect of static fields of 60–200 mT on the proliferation of the endothelium was revealed [6, 7].

At the same time, the chains of biogenic magnetic nanoparticles (BMNs) in the capillary walls are the most sensitive biophysical target for the influence of the magnetic field on organisms [17–19]. The magnetic field influences on membrane-bound magnetic nanoparticles and creates mechanical forces and, accordingly, the wall shear stress, which controls the mechanosensitive ion channels [18, 19]. At the same time, there are methods of controlling mechanosensitive ion channels using artificial magnetic nanoparticles (MNPs) attached to the cell membrane. For example, a magnetic particle-based

technique has been developed that allows highly localized mechanical forces to be applied directly to specific regions of an ion channel structure, and it has been demonstrated that this approach can be used to directly and selectively activate a mechanosensitive ion channel, namely TREK-1 [20]. In addition, functionalized magnetic nanoparticles targeting mechanosensitive integrins or TREK-1 ion channels have demonstrated that active targeting can stimulate intracellular calcium levels compared to controls [21]. Also, magnetic iron oxide nanoparticles can stimulate the mechanosensitive ion channel Piezo1 through a magneto-mechanical mechanism [22] and stimulate the epidermal growth factor receptor EGFR. The non-selective cation channel TRPV4, present in various cell types, can be activated by magneto-mechanical or electromagnetic stimulation using 100 nm MNPs coated with proteins or MNPs in the form of magnetic nanodiscs with a size of 226 nm, respectively. Induction of intracellular calcium flux through mechanical activation of mechanosensitive N-type Ca^{2+} channels can be induced in neurons grown on substrates that create high-gradient local fields in the vicinity of 100 nm MNPs coated with starch under the influence of the magnetic field of a permanent magnet.

Endothelial cells as participants in angiogenesis choose their phenotype as tip cells (leading, migrating) or stem cells (following) [23]. It has been experimentally found and theoretically modeled that rapid oscillations of calcium concentration inside the cell play a key role in controlling phenotype selection and possible vascular architecture [23]. In addition, the control of oscillations in the intracellular concentration of calcium in endothelial cells is known due to the wall shear stress caused by blood flow, which controls mechanosensitive calcium ion channels [24]. At the same time, mechanosensitive ion channels are expressed in endothelial cells and play an important role in them [25–30].

In this work, the task of modeling of the dynamics of the intracellular concentration of calcium in endothelial cells is solved due to the influence of external magnetic fields on artificial or biogenic magnetic nanoparticles embedded in the cell membrane, the creation of a corresponding "magnetic" wall shear stress, which in turn activates mechanosensitive ionic calcium channels [18, 19]. As a result, the end result of such modeling is the control of endothelial cell phenotype selection in magnetic fields. The results of this work contribute to the explanation of conflicting literature data on the influence of moderate static and low-frequency magnetic fields on angiogenesis, taking into account the presence of biogenic magnetic nanoparticles in the capillary walls [17, 18] well as achieving a controlled effect on the proliferation of endothelial cells using artificial magnetic nanoparticles for controlling mechanosensitive calcium ion channels under the influence of magnetic fields.

Methods

To solve the problem, the "magnetic" wall shear stress was calculated which arises as a result of the influence of an external magnetic field on magnetic nanoparticles embedded in the cell membrane and which controls the mechanosensitive calcium ion channels [18, 19]. There are technologies for manufacturing magnetic nanoparticles with a wide range of potential applications. Magnetic nanoparticles, crucial for biomedical applications, are synthesized through methods like co-precipitation, thermal decomposition, hydrothermal synthesis, and sol-gel synthesis, enabling control over size and magnetic properties. Post-synthesis, they undergo functionalization with materials like dextran, polyethylene glycol, or silica to stabilize, prevent aggregation, and facilitate conjugation with targeting agents, drugs, or imaging labels. Conjugation allows binding to specific cells or tissues, drug or gene delivery, and imaging enhancement. Following functionalization, characterization ensures desired properties through techniques like dynamic light scattering, transmission electron microscopy, and magnetic measurements, followed by purification to remove unbound agents. *In vitro* applications include cell imaging, drug delivery, and genetic manipulation, while *in vivo* applications encompass targeted drug delivery, magnetic resonance imaging contrast enhancement, and cancer hyperthermia treatment, among others [31]. For example, in the Henstock *et al.* experiment, nanoparticles were conjugated with antibodies targeting the TREK1 ion channel on the surface of human mesenchymal stem cells, and manipulation was performed using a specially designed vertical oscillating magnetic bioreactor that generated an oscillating magnetic field. In the Gregurec *et al.* experiment, colloidal synthesized magnetite nanodisks were attached to cell explants of spinal ganglia to create a torque on the nanodisks and activate the mechanosensitive cation channel TRPV4 under the influence of weak and slow magnetic fields. In the Hao *et al.* study, it was noted that nanodeformation of magnetically sensitive biomaterial (MC3T3-E1 mouse cells exposed to culture media filled with a composite ma-

terial of iron oxide nanoparticles) under the influence of a static magnetic field can create mechanical stress to further stimulate the mechanosensitive protein Piezo1 and accelerate osteogenesis.

Equations and methods of magnetostatics were used to make such a calculation. Then, numerical modeling of oscillations in intracellular calcium concentration in endothelial cells and determination of their final phenotype was carried out taking into account the "magnetic" wall shear stress [18, 19]. The modeling is based on the mathematical model of the work [23], which describes oscillations in the intracellular concentration of calcium in endothelial cells and their role in the choice of cell phenotype. Thus, in this work, two additional factors of influence on cells are added to the model of intracellular calcium concentration dynamics of work [18, 19, 23]: the presence or absence of a chain of MNPs on the cell membrane and an external magnetic field.

To achieve the controlled effect, the frequencies of alternating gradient or homogeneous magnetic fields must correspond to the calcium oscillation modes, which positively correlate with the specific frequencies and durations of influence of the decoding enzymes involved in the physiological process. To modulate calcium oscillations, frequencies of magnetic fields are selected that have a resonant character [19].

The python programming language and python programming language packages: scipy, py-pde, matplotlib were used for numerical simulations.

Results

The model of the paper [23] of dynamics of the intracellular Ca^{2+} concentration includes the interaction between IP3R – the IP3 receptor (inositol 1,4,5-trisphosphate) and the SERCA pump (sarco/endoplasmic reticulum Ca^{2+}-ATPase), as well as between factors related to angiogenesis: DLL4 (delta-like ligand 4/transmembrane protein that activates the Notch pathway), Notch (Notch proteins are a family of transmembrane proteins of the type 1, which form the main component of the Notch signaling pathway, which is highly conserved in animals), NICD (Notch intracellular domain) and HE (hairy and enhancer-of-split family of proteins-split) (Figs. 1 and 2, Table 1). DLL4 and Notch proteins are transmembrane proteins that interact with each other to create the DLL-Notch complex, which is also included in the model in the work [23]. In addition, HE family proteins mediate changes in Ca^{2+} concentration through negative feedback, and DLL4 protein expression is associated with calcium concentration.

In the paper [23], DLL4 protein concentration is considered as the only determinant of endothelial cell phenotype, i.e. the phenotype of endothelial cells depends only on the concentration DLL4. The specific role of the DLL4 protein is in the selection of tip cells during angiogenesis, which leads to the corresponding branching of the vasculature [32]. DLL4 protein expression is very low in normal adult endothelium, its increased expression has been observed in the tumor-associated endothelium of several cancers, including bladder, breast, colon, kidney, and brain, while expression is much lower or absent in the adjacent normal vasculature [32]. The DLL4 protein is important for pathological angiogenesis and is overexpressed in human tumors, often in association with markers of inflammation, hypoxia, and angiogenesis [32]. DLL4 is a Notch1 ligand required for embryonic vascular development and arteriogenesis [33]. Increased expression of DLL4 in endothelial cells reduces the formation of metastases and improves the accumulation of drugs during chemotherapy in the primary tumor [34]. Overexpression of DLL4 promotes vessel maturation and stabilization of the tumor vasculature by reducing its ability of remodeling and, thus, reduces the risk of developing resistance to therapy, as well as improves drug de-

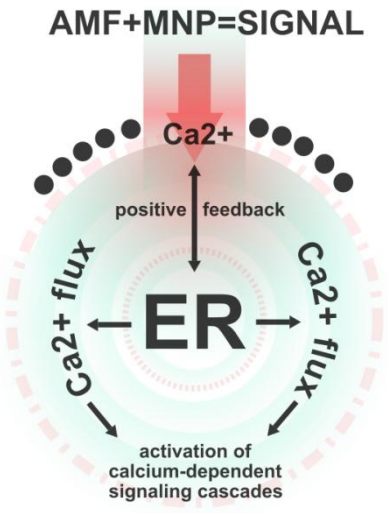

Figure 1: The schematic image of the key mechanisms at play: an increase in the concentration of calcium in the cell due to its entry through ion channels leads to a calcium-dependent release of calcium from the endoplasmic reticulum. This is a positive feedback process. Calcium decoders read the signal and trigger a cascade of calcium-dependent processes. The notations are introduced: ER is endoplasmic reticulum, AMF is alternative magnetic field, MNP are magnetic nanoparticles

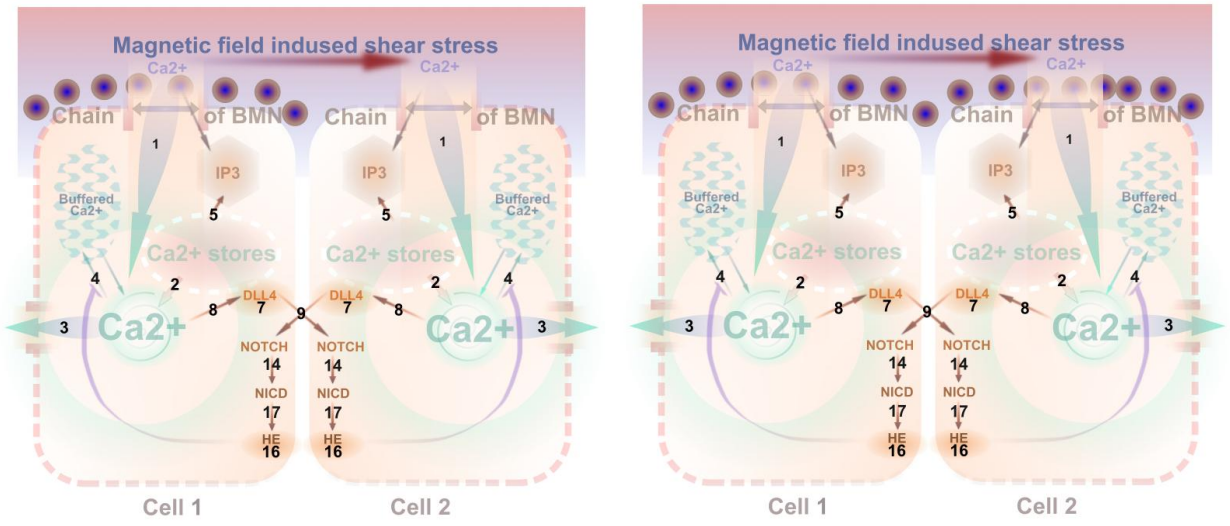

Figure 2: Schematic representation of the two-cell model with an explanation of the relevant factors and the interactions between them: (a) MNP chain on the membrane of one of the two cells; (b) MNP chain on the membrane of both cells. Dynamic model variables are the concentrations of Ca^{2+}, IP3, DLL4, NOTCH, DLL 4-NOTCH complex, NICD, HE (Table 2). The stream numbers next to the arrows correspond to the row numbers of Table 2

livery to the tumor [34]. Inhibition of DLL4 suppresses experimental tumor growth by inducing nonp roductive, misregulated angiogenesis [32]. Inhibition of DLL4/Notch signaling leads to excessive, dysfunctional vascular proliferation and significant inhibition of tumor growth. Therefore, new therapeutic strategies are being developed, such as inhibition of DLL4 [33]. Study of genetic deletion showed that haploinsufficiency DLL4, a transmembrane ligand for the Notch family of receptors, leads to large vascular defects and embryonic lethality [35].

Thus, there was a need to regulate the level of expression of DLL4, including both its increase and suppression. Debir's paper [23] presents seven interrelated equations of the dynamics of intracellular calcium concentrations, the fraction of IP3 receptors not inactivated by calcium, and the concentrations of DLL4, Notch, the DLL4-Notch complex, NICD, and HE. These equations include dimensionless dynamic variables, dimensionless constants, and dimensionless time (Fig. 2). The first three equations in paper [23] are formulated on the basis of Atri's model [36], where these equations are presented in dimensional form. The next four equations of the system of seven dynamic equations in Debir's paper [23] are formulated based on the paper by Venkatraman [37], where these equations are also presented in dimensional form and in other notations. The formulas and coefficients of the transition from the dimensional dynamic variables and constants of the papers by Atri [36] and Venkatraman [37] to the corresponding dimensionless quantities in the paper by Debir [23] are presented in Table 2 and Table 3. In Tables 2 and 3, all dimensionless variables and constants that are used in the paper by Debir [23], denoted by letters with a stroke, and all relevant dimensional variables and constants from the papers by Atri [36] and Venkatraman [37] are denoted without a stroke.

The dimensional equations of the papers by Atri [37] and Venkatraman [37] (see below, formulas (1.1)–(7.2) represent 14 equations for two cells. The indices $i = 1, j = 2$ for the first 7 equations, the indices $i = 2, j = 1$ for the next 7 equations represent numbers the flows (Table 2) and dynamic variables (Table 1) that refer to the first $(i = 1)$ and second $(j = 2)$ cell respectively. The expressions for the fluxes are given in Table 2, the values of the dimensional constants of the model are given in Table 3.

Equations describing the first cell taking into account its interaction with the second cell (1.1), (2.1), (3.1), (4.1), (5.1), (6.1), and (7.1) reflect the dynamics of concentration of calcium in the cytosol, the part of IP3 receptors not inactivated by calcium, the concentrations of DLL4, Notch, DLL-Notch complex, NICD and HE proteins, respectively:

Table 1: Dynamic variables in the model of calcium concentration dynamics

Dynamic variable	Dimensional notation	Relationship between dimensional and dimensionless variable	Dimensionless notation
Time	t, s	$t = \tau_n t'$	t'
Part of IP3 receptors not inactivated by calcium	n	$n = n'$	n'
Ca^{2+} in the cytosol (calcium concentration in the cytosol)	C, μM	$C = k_1 C'$	C'
DLL4 concentration	ν, conc	$v' = k_9' v$	v'
Concentration of Notch	w, conc	$w' = k_9' w$	w'
Concentration of the DLL-Notch complex	x, conc	$x' = k_9' x$	x'
Concentration of NICD in the cell	y, conc	$y' = k_9' y$	y'
Concentration of Hairy and Enhancer-of-split family proteins in the cell	z, conc	$z' = k_9' z$	z'

Note. The notation "*conc*" means concentration units introduced in [38]. Because of the lack of experimental measurements of protein concentrations, we use concentration units (conc = cu.) as a unit to represent relative protein concentrations in the model, as suggested in [38]. Cell number index for each dynamic variable and each constant is omitted in the table to make the notation less cumbersome.

$$\frac{dC_1}{dt} = J_{channel1} - J_{pump1} - v_{31} + J_{WSS1}. \quad (1.1)$$

Equation (1.1) after substituting the fluxes (in other words, the rate of change of the Ca^{2+} concentration in the cytosol) from Table 2 is written in the form:

$$\frac{dC_1}{dt} = k_{flux}\mu([IP_3])n_1\left(b + \frac{v_1 C_1}{k_1 + C_1}\right) - \frac{\gamma C_1}{k_\gamma + C_1} - \zeta z_1 C_1 + \frac{q_{\max 1}}{1 + \alpha \exp\left(-\frac{f_e W(\tau)}{kT_e N}\right)}, \quad (1.2)$$

$$\tau_n \frac{dn_1}{dt} = n_\infty(C_1) - n_{C1} - n_1, \quad (2.1)$$

where $n_\infty(C_1) = 1 - \frac{C_1^2}{k_2^2 + C_1^2}$, C_1 is the concentration of calcium in the cytosol in the first cell (left cell in Fig. 1); n_1 is the part of IP3 receptors not inactivated by calcium in the first cell.

Equation (2.1) after substituting the fluxes (in other words, the rates of change of the fraction of IP3 receptors not inactivated by calcium) from Table 2 is written in the form:

$$\tau_n \frac{dn_1}{dt} = 1 - \frac{C_1^2}{k_2^2 + C_1^2} - \frac{C_1^2}{1 + C_1^2} - n_1. \quad (2.2)$$

Here we follow the logic of the paper [23] and consider the concentration of DLL4 as the only determinant of the of the cell phenotype, that is, the phenotype of endothelial cells depends only on the concentration DLL4.

$$\frac{dv_1}{dt} = \beta + v_{41} - v_{512} + v_{62} - \varphi v_1. \quad (3.1)$$

Equation (3.1) after substituting flows (in other words, rates of change in DLL4 concentration) from Table 2 is written in the form:

$$\frac{dv_1}{dt} = \beta + \Theta \frac{C_1^2}{k_4^2 + C_1^2} - k_2 v_1 w_2 + k_{-2} x_2 - \varphi v_1. \quad (3.2)$$

The right part of equation (3.2) reflects the rate of change in the concentration of DLL4, namely the first term – the basal expression of DLL4 (β), the second is the expression of the DLL4 gene dependent on the concentration of Ca^{2+}, the third is the formation of the complex of the DLL4 protein with the Notch protein of the neighboring cell, the fourth is the dissociation of the complex DLL4-Notch (v_{62}) and the fifth is DLL4 degradation (φv_1).

$$\frac{dw_1}{dt} = -v_{521} + k_{-2} x_2 - \varphi w_1. \quad (4.1)$$

Table 2: Fluxes in the calcium dynamics model

Row	Physical quantity	Formula/description
1	Rate of flow of Ca^{2+} into the cell through the mechanosensitive ion channel depending on the wall shear stress τ [24]	$J_{WSSi} = \frac{q_{\max}}{1 + \alpha \exp\left(-\frac{f_e W(\tau)}{kT_e N}\right)}$, $J'_{WSSi} = \frac{q'_{max}}{1 + \alpha \exp\left(-\frac{f_e W(\tau)}{kT_e N}\right)}$

where τ is the applied wall shear stress, N is the density of channels per unit area of the cell membrane, k is the Boltzmann constant, T_e is the absolute temperature, α ($\alpha \geq 0$) is a measure of the probability that the channel is in an open state in the case without of the applied wall shear stress, namely $(1+\alpha)^{-1}$ is the probability that the channel is in the open state in the case of no load, that is, when $W = 0$, f_e ($0 \leq f_e \leq 1$) is the fraction of membrane energy that affects Ca^{2+} channels sensitive to wall shear stress.

The energy density function of elastic deformation for a two-dimensional membrane has the following form [38, 39]:

$$W(\tau) = \frac{[\varepsilon' \tau l + \sqrt{16\delta^2 + \varepsilon'^2 \tau^2 l^2} - 4\delta]^2}{8[\varepsilon' \tau l + \sqrt{16\delta^2 + \varepsilon'^2 \tau^2 l^2}]},$$

where ε' is the fraction of the load influencing on the submembrane structure, δ is the shear modulus of the membrane, l is the cell length in the direction of the force that creates the wall shear stress.

To take into account the effects of the magnetic field, we present the shear stress caused by the magnetic field as the sum of the shear stress caused by the blood flow: $\tau = \tau_h + \tau_{magn}$ [19], where τ_h is the shear stress on the endothelial cell membrane caused by the hydrodynamic blood flow (typical values: $\tau_h = 1$ Pa for the artery and $\tau_h = 0.1$ Pa [40] for a capillary), τ_{magn} – wall shear stress caused by magnetic forces acting on a chain of magnetic nanoparticles embedded in the cell membrane. In addition, we consider the wall shear stresses caused by gradient and uniform MPs.

The wall shear stress is calculated by the formula $\tau_{magn} = \frac{F_\tau}{N\pi r^2}$, where F_τ is the component of the gradient magnetic force in the plane of the membrane, r is the radius of the magnetic nanoparticle [18, 19]. In the gradient magnetic field, the shear stress has the form $\tau_{magn} = \frac{4rMG\sin\theta_0}{3} \cdot \cos(\omega t)$ [18, 19], where M is the magnetization of a magnetic nanoparticle (which is a function of the applied magnetic field), $G = \left|\frac{\partial \vec{B}}{\partial z}\right|$, θ_0 – the angle between $\frac{\partial \vec{B}}{\partial z}$ and the normal to the plane of the membrane in the case where the z axis is chosen in the direction of magnetization $\vec{M}$ (Fig. 3a) [18, 19]. The parameter G characterizes the value of the gradient of the magnetic field and is considered as an oscillating harmonic function, the case of a constant magnetic field gradient is described at $\omega = 0$ [19].

In the case of a uniform magnetic field,

$$\tau_{magn} = \frac{\pi}{6N} MB\sin\theta sin\gamma \cdot \cos(\omega t)\ [18, 19],$$

where θ is the angle between the normal to the cell membrane and the direction of the magnetic field, γ is the angle between the in-plane component of the magnetic field and the magnetization of the chain of magnetic nanoparticles (Fig. 3b) [18, 19]. In the general case, the induction of a uniform magnetic field B in the previous formula is considered as an oscillating harmonic function, while $\omega = 0$ for a static magnetic field [19].

Table 2 continuation

Row	Physical quantity	Formula/description	
2	Flow of Ca^{2+} from the endoplasmic reticulum, mediated by the IP3 receptor (the rate of release of Ca^{2+} from the endoplasmic reticulum)	$J_{channel} = k_{flux}\mu([IP_3])n\left(b + \frac{v_1 C}{k_1 + C}\right)$, $\mu([IP_3]) = \mu_0 + \frac{\mu_1[IP_3]}{k_\mu + [IP_3]}$, μ – concentration of $([IP_3])$, ν – concentration of DLL4	$q_{rel} = k_1'\mu' n'\left(\frac{b' + C'}{1 + C'}\right)$
3	Calcium efflux from the cytoplasm to the outside of the cell (calcium efflux rate)	$J_{pump} = \frac{\gamma C}{k_\gamma + C}$	$q_{out} = k_2' \cdot \frac{C'}{k_3' + C'}$
4	Negative feedback relationship between the concentration of proteins of the HE family and the concentration of calcium	$v_3 = \zeta z C$	$q_{HE} = \zeta' z' C'$
5	Calcium-mediated inactivation of the IP3 receptor	$\frac{C^2}{K_2^2 + C^2}$	$n_C = \frac{C'^2}{1 + C'^2}$
6	Part of IP3 receptors not inactivated by calcium	n	n'
7	Basal expression of DLL4 protein. The basal expression level is the level of mRNA or protein expression. Basically, it's how much a cell or tissue makes a certain mRNA or protein under normal conditions. It is a level that can be compared between different types of cells or tissues, or one can compare the basal level of expression with the level of expression caused by some stimulus	β	β'
8	Calcium-mediated DLL4 gene expression	$\Theta \frac{C^2}{k_4^2 + C^2}$	$v_4' = \Theta' \cdot \frac{C'^2}{k_4'^2 + C'^2}$
9	Association of the DLL4 protein from a neighboring cell with Notch. Association is the joining of molecules or ions into groups under the influence of the forces of intermolecular interaction of an electrical nature	$v_{5ij} = k_2 v_i w_j$	$v_{5ij}' = k_5' v_i' w_j'$

Ending of Table 2

Row	Physical quantity	Formula/description	
10	Dissociation of the DLL-Notch complex. Dissociation is a chemical process of breaking down molecules into simpler molecules, atoms, atomic groups, or ions. The opposite process is association	$v_6 = k_{-2}x$	$v_6' = k_6'x'$
11	Degradation of DLL4	φv	$k_7'v'$
12	Notch degradation	φw	$k_7'w'$
13	Degradation of the DLL-Notch complex	φx	$k_7'x'$
14	Catalysis of the DLL-Notch complex	$v_7 = k_4x$	$v_7' = k_8'x'$
15	Degradation of NICD	φy	$k_7'y'$
16	Basal secretion of HE factor	β	β'
17	NICD-mediated HE gene expression	$v_8 = \frac{\theta y^2}{y^2+1}$	$v_8' = \theta' \frac{y'^2}{y'^2 + k_9'^2}$
18	Degradation of HE	φz	$k_7'z'$

Note. The cell number index for each flux, each dynamic variable, and each constant (except those included in the expressions v_{5ij} and v_{5ij}') are omitted in the table to make the notation less cumbersome.

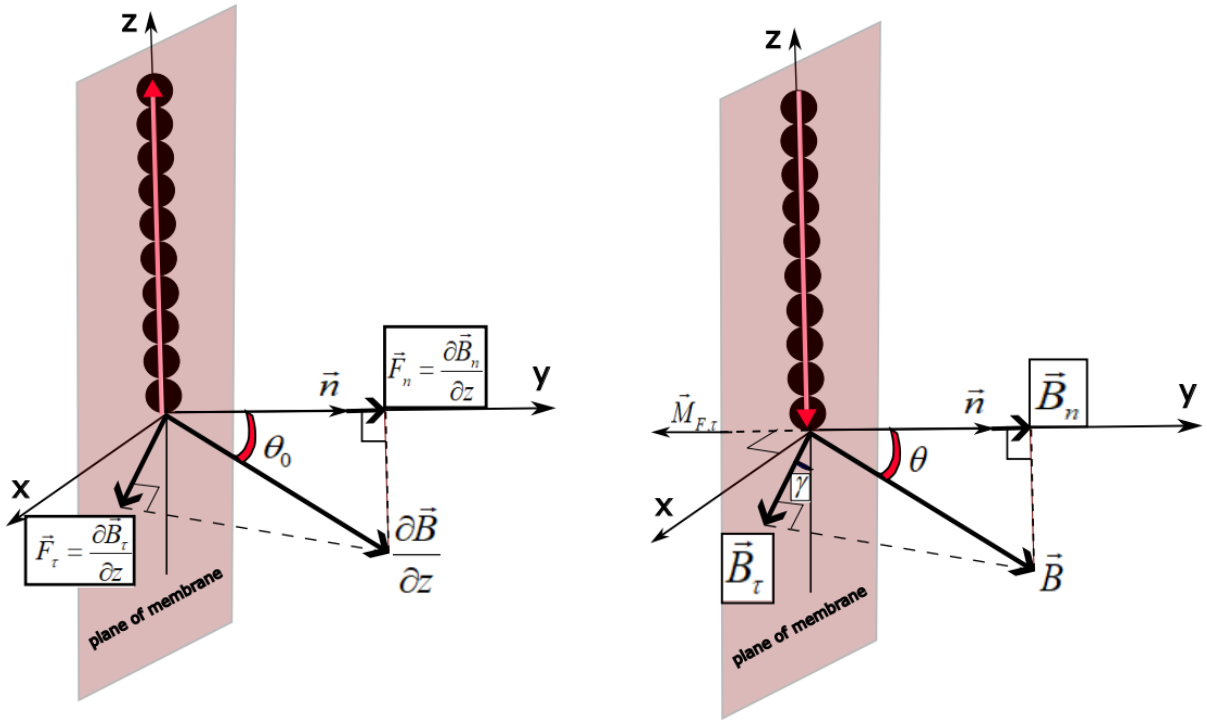

Figure 3: Scheme of calculation of wall shear stress under the influence of the MNP chain under (a) gradient magnetic field [18, 19]; (b) uniform magnetic field [18, 19]

Table 3: Parameters of the calcium concentration dynamics model

Parameter used in the model for calcium concentration dynamics	Value of dimensional parameters	Relationship between dimensional and dimensionless parameters	Dimensionless parameter values
Maximum rate of Ca^{2+} influx caused by wall membrane shear stress (WSS)	$q_{\max} = 17.6\ \mu Ms^{-1}$ [24]	$q'_{\max}{}^{(Plank)} = \frac{q_{\max} T^{(Plank)}}{K_4^{(Plank)}}$ $q'_{\max} = \frac{q_{\max}\tau_n}{k_1} = \frac{q'_{\max}{}^{(Plank)} K_4^{(Plank)} \tau_n}{T^{(Plank)} k_1}$ $K_4^{(Plank)} = 0.32\ \mu M$ [24] $T^{(Plank)} = 500\ s$ [24] $\tau_n = 2\ s$ [37] $k_1 = 0.7\ \mu M$ [37]	$q'_{\max}{}^{(Plank)} = 27500$ in the Plank model [24] $q'_{\max} = 50.3$ in the Debir model [23]
Part of the load (i.e. shear stress) influencing on the submembrane structure			$\varepsilon' = 0.1$ [24]
Fraction of the membrane strain energy that gates the calcium ion channel			$f'_e = 0.0134$ [24]
Surface density of Ca^{2+} channels	$N = 10^{12} m^{-2}$ [24]		
Boltzmann constant	$k = 1.3807 \cdot 10^{-23} kg \cdot m^2 s^{-2} K^{-1}$		
Temperature	$T_e = 310\ K$		
Membrane shear modulus	$\delta = 10^{-5}\ kg \cdot s^{-2}$ [24]		
Length of the cell in the direction of the force that produces wall shear stress	$l = 3.5 \cdot 10^{-5}\ m$ [24]		
Concentration of IP3 (the fraction of IP3Rs in which the domain of IP3 binding is activated)	$\mu([IP_3])$ $0 \le \mu([IP_3]) \le 1$	$\mu([IP_3]) = \mu'$	$0 \le \mu' \le 1$
Basal expression of protein genes	$\beta = 0.001\ s^{-1}$ [38]	$\beta' = \beta\tau_n k'_9$	$\beta' = 0.001$ [23]
Rate of NICD production	$\theta = 0.1 conc.s^{-1}$ [38]	$\theta' = \tau_n k'_9 \theta$	$\theta' = 0.1$ [23]
DLL4 production rate	$\Theta = 1.5 conc.s^{-1}$	$\Theta' = \Theta\tau_n k'_9$	$\Theta' = 1.5$ [23]
Parameter in expression for inactivation of the IP3 receptor by Ca	$K_2 = 0.7\ \mu M$ [37]		
Indicator of negative feedback of HE with Ca	$\zeta = 0.15 conc^{-1} \cdot s^{-1}$	$\zeta' = \frac{\zeta\tau_n}{k'_9}$	$\zeta' = 0.6$ [23]
Basal current through IP3R	$b = 0.111$ [37] $v_1 = 0.889$ [37]	$b' = \frac{b}{b + v_1}$ $b + v_1 = 1$	$b' = 0.111$ [23]

Ending of Table 3

Parameter used in the model for calcium concentration dynamics	Value of dimensional parameters	Relationship between dimensional and dimensionless parameters	Dimensionless parameter values
Maximum total flow of Ca^{2+} through IP3R	$k_{flux} = 8.1\ \mu Ms^{-1}$ [37] $k_1 = 0.7\ \mu M$ [37] $b = 0.111$ [37] $v_1 = 0.889$ [37]	$k_1' = \frac{\tau_n k_{flux}}{k_1(b + v_1)}$	$k_1' = 23.1$ [23]
Maximum rate of Ca^{2+} pumping from the cytosol	$\gamma = 2.0\ \mu Ms^{-1}$ [37] $k_1 = 0.7\ \mu M$ [37]	$k_2' = \frac{\gamma\tau_n}{k_1}$	$k_2' = 5.7$ [23]
Half of the maximum rate of Ca^{2+} pumping from the cytosol	$k_\gamma = 0.1\ \mu M$ [37] $k_1 = 0.7\ \mu M$ [37]	$k_3' = \frac{k_y}{k_1}$	$k_3' = 0.14$ [23]
Half of the maximum production speed of DLL4	$k_4 = 0.98\ \mu M \approx 1\ \mu M$ [38] $k_1 = 0.7\ \mu M$ [37]	$k_4' = \frac{k_4}{k_1}$	$k_4' = 1.4$ [23]
Association rate for the dn complex	$k_2 = 0.1 conc \cdot s^{-1}$	$k_5' = k_2\tau_n / k_9'$	$k_5' = 0.4$ [23]
	$k_2 = 0.001 conc \cdot s^{-1}$ [38]		$k_5' = 0.004$
Rate of dissociation of the dn complex	$k_{-2} = 0.001 conc \cdot s^{-1}$	$k_6' = \tau_n k_{-2}$	$k_6' = 0.002$ [23]
	$k_{-2} = 0.1 conc \cdot s^{-1}$ [38]		$k_6' = 0.2$
Rate of protein degradation	$\varphi = 0.005\ s^{-1}$	$k_7' = \varphi\tau_n$	$k_7' = 0.01$ [23]
	$\varphi = 0.001\ s^{-1}$ [38]		$k_7' = 0.002$
Rate of catalysis of the dn complex	$k_4 = 0.1\ s^{-1}$ [38]	$k_8' = \tau_n k_4$	$k_8' = 0.2$ [23]
Half of the maximum production rate of NICD			$k_9' = 0.5$

Note. The cell number index for each dynamic variable and each constant is omitted in the table to make the notation less cumbersome.

Equation (4.1) after substituting the flows (in other words, the rates of change of Notch concentration) from Table 2 is written in the form:

$$\frac{dw_1}{dt} = -k_2 v_2 w_1 + k_{-2} x_2 - \varphi w_1, \qquad (4.2)$$

where v_1, w_1 and x_1 describe the concentrations of DLL4, Notch, and the DLL-Notch complex, respectively.

The corresponding rates in the right-hand side of equation (4.2) have the following meaning: the first term is the association of the DLL4 protein of the neighboring cell with the Notch protein of the first cell, the second term is the dissociation of the DLL-Notch complex, and the third term is the degradation of the Notch protein.

$$\frac{dx_1}{dt} = v_{521} - k_{-2} x_1 - \varphi x_1. \qquad (5.1)$$

Equation (5.1) after substituting the flows (in other words, the rates of change in the concentration of the DLL-Notch complex) from Table 2 is written in the form:

$$\frac{dx_1}{dt} = k_2 v_2 w_1 - k_{-2} x_1 - \varphi x_1. \qquad (5.2)$$

In addition, the terms on the right side of equation (5.2) have the following meaning: the first term corresponds to the binding of the DLL4 protein of the neighboring cell with the Notch protein of the first cell, the second term corresponds to the dissociation of the DLL-Notch complex and the degradation of the DLL-Notch complex.

After signal transmission between neighboring cells through the formation of the DLL4-Notch complex, the equations depicting the secretion of HE family proteins in the first cell caused by NICD proteins are given by formulas (6.1), (7.1)

$$\frac{\mathrm{d}y_1}{\mathrm{d}t} = v_{71} - \varphi y_1 . \qquad (6.1)$$

Equation (6.1) after substituting flows (in other words, rates of change of NICD concentration) from Table 2 is written in the form:

$$\frac{\mathrm{d}y_1}{\mathrm{d}t} = k_4 x_1 - \varphi y_1 . \qquad (6.2)$$

The terms on the right side of equation (6.2) have the following meaning: the first describes the catalysis of the DLL-Notch complex, the second describes the degradation of NICD.

$$\frac{\mathrm{d}z_1}{\mathrm{d}t} = \beta + v_{81} - \varphi z_1 . \qquad (7.1)$$

Equation (7.1) after substituting flows (in other words, rates of change of NICD concentration) from Table 2 is written in the form:

$$\frac{\mathrm{d}z_1}{\mathrm{d}t} = \beta + \frac{\theta y_1^2}{y_1^2 + 1} - \varphi z_1 . \qquad (7.2)$$

The dynamic variables y_1 and z_1 in equations (6.1), (6.2), (6.3), (6.4) describe the concentrations of NICD and HE in the first cell. The terms on the right-hand side of equation (7.2) are as follows: the first term is the basal secretion of the HE factor, the second term is the expression of the HE gene, depending on the concentration of NICD, and the third term is the degradation of HE.

Equations describing the second cell taking into account its interaction with the first cell (8.1), (9.1), (10.1), (11.1), (12.1), (13.1), and (14.1) reflect the dynamics of concentration of calcium in the cytosol, the part of IP3 receptors not inactivated by calcium, the concentrations of DLL4, Notch, DLL-Notch complex, NICD and HE proteins, respectively:

$$\frac{dC_2}{dt} = J_{channel2} - J_{pump2} - v_{32} + J_{WSS2} . \qquad (8.1)$$

Equation (8.1) after substituting the flows (in other words, the rates of change of Ca^{2+} concentration in the cytosol) from Table 2 is written in the form:

$$\frac{dC_2}{dt} = k_{flux}\mu([IP_3])n_2\left(b + \frac{v_1 C_2}{k_1 + C_2}\right) - \frac{\gamma C_2}{k_\gamma + C_2} - \zeta z_2 C_2 + \frac{q_{\max 2}}{1 + \alpha \exp\left(-\frac{f_e W(\tau)}{kT_e N}\right)} . \qquad (8.2)$$

$$\tau_n \frac{\mathrm{d}n_2}{\mathrm{d}t} = n_\infty(C_2) - n_{C2} - n_2 , \qquad (9.1)$$

where $n_\infty(C_2) = 1 - \frac{C_2^2}{k_2^2 + C_2^2}$, C_2 is the concentration of calcium in the cytosol in the second cell (the right cell in Fig. 1); n_2 is the part of IP3 receptors not inactivated by calcium in the second cell.

Equation (9.1) after substituting the fluxes (in other words, the rates of change of the fraction of IP3 receptors not inactivated by calcium) from Table 2 is written in the form:

$$\tau_n \frac{\mathrm{d}n_2}{\mathrm{d}t} = 1 - \frac{C_2^2}{k_2^2 + C_2^2} - \frac{C_2^2}{1 + C_2^2} - n_2 . \qquad (9.2)$$

Here we also follow the same logic and consider DLL4 concentration as the sole determinant of cell phenotype expression.

$$\frac{\mathrm{d}v_2}{\mathrm{d}t} = \beta + v_{42} - v_{521} + v_{61} - \varphi v_2 . \qquad (10.1)$$

Equation (10.1) after substituting flows (in other words, rates of change in DLL4 concentration) from Table 2 is written in the form:

$$\frac{\mathrm{d}v_2}{\mathrm{d}t} = \beta + \Theta \frac{{C_2}^2}{k_4^2 + {C_2}^2} - k_2 v_2 w_1 + k_{-2} x_1 - \varphi v_2 . \qquad (10.2)$$

The right-hand side of equation (10.2) reflects the rate of change in the concentration of DLL4, namely the first term is the basal expression of DLL4, the second term is the expression of the DLL4 gene dependent on the concentration of Ca^{2+}, the third term is the formation of the DLL4 protein complex with the Notch protein of the neighboring cell, the fourth term is the dissociation of the DLL4- Notch complex and the fifth term is DLL4 degradation.

$$\frac{\mathrm{d}w_2}{\mathrm{d}t} = -v_{512} + k_{-2} x_1 - \varphi w_2 . \qquad (11.1)$$

Equation (10.1) after substituting the flows (in other words, the rates of change of Notch concentration) from Table 2 is written in the form:

$$\frac{dw_2}{dt} = -k_2 v_1 w_2 + k_{-2} x_1 - \varphi w_2 . \quad (11.2)$$

The corresponding rates in the right-hand side of equation (11.2) have the following meaning: the first term is the association of the DLL4 protein of the neighboring cell with the Notch protein of the second cell, the second term is the dissociation of the DLL-Notch complex, and the third term is the degradation of the Notch protein.

$$\frac{dx_2}{dt} = v_{512} - k_{-2} x_2 - \varphi x_2 , \quad (12.1)$$

where v_2, w_2 and x_2 describe the concentrations of DLL4, Notch and DLL-Notch complex in the second cell, respectively.

Equation (12.1) after substituting the flows (in other words, the rates of change in the concentration of the DLL-Notch complex) from Table 2 is written in the form:

$$\frac{dx_2}{dt} = k_2 v_1 w_2 - k_{-2} x_2 - \varphi x_2 . \quad (12.2)$$

In addition, the terms on the right side of equation (12.2) have the following meaning: the first term corresponds to the binding of the DLL4 protein of the neighboring cell with the Notch protein of the second cell, the second term corresponds to the dissociation of the DLL-Notch complex and the degradation of the DLL-Notch complex.

After signaling between neighboring cells through the formation of the DLL4-Notch complex, the equations depicting the secretion of HE family proteins in the second cell caused by NICD proteins are given by formulas (13.1), (14.1).

$$\frac{dy_2}{dt} = v_{72} - \varphi y_2 . \quad (13.1)$$

Equation (13.1) after substituting flows (in other words, rates of change of NICD concentration) from Table 2 is written in the form:

$$\frac{dy_2}{dt} = k_4 x_2 - \varphi y_2 . \quad (13.2)$$

The terms on the right side of equation (13.2) have the following meaning: the first term describes the catalysis of the DLL-Notch complex, the second term describes the degradation of NICD.

$$\frac{dz_2}{dt} = \beta + v_{82} - \varphi z_2 . \quad (14.1)$$

Equation (14.1) after substituting flows (in other words, rates of change of NICD concentration) from Table 2 is written in the form:

$$\frac{dz_2}{dt} = \beta + \frac{\theta y_2^2}{y_2^2 + 1} - \varphi z_2 , \quad (14.2)$$

where y_2 and z_2 describe the concentrations of NICD and HE in the second cell. The terms on the right-hand side of equation (14.2) are as follows: the first term is the basal secretion of the HE factor, the second term is the expression of the HE gene, dependent on the concentration of NICD, and the third term is the degradation of HE.

The corresponding dimensionless equations [23, 36, 37] (here and further a dash indicates that the flow or dynamic variable is dimensionless) are given by the formulas (1.1)–(7.2) given below:

$$\frac{dC_1'}{dt'} = q_{rel}{}'_1 - q_{out}{}'_1 - q_{HE}{}'_1 + J'_{WSS} , \quad (1.1a)$$

$$\frac{dC_1'}{dt'} = k_1' \, \mu' n_1' \left(\frac{b' + C_1'}{1 + C_1'} \right) - k_2' \cdot \frac{C_1'}{k_3' + C_1'} - \zeta' z_1' \, C_1' + \frac{q'_{max1}}{1 + \alpha \exp\left(- \frac{f_e W(\tau)}{k T_e N} \right)}, \quad (1.1b)$$

$$\frac{dn_1'}{dt'} = 1 - n'_{C1} n_1' , \quad (1.2a)$$

$$\frac{dn_1'}{dt'} = 1 - \frac{C_1'^2}{1 + C_1'^2} - n_1' , \quad (1.2b)$$

$$\frac{dv_1'}{dt'} = \beta' + v'_{41} - v'_{512} + v'_{62} - k_7' v_1' , \quad (1.3a)$$

$$\frac{dv_1'}{dt'} = \beta' + \Theta' \cdot \frac{C_1'^2}{k_4'^2 + C_1'^2} - k_5' v_1' w_2' + k_6' x_1' - k_7' v_1' , \quad (1.3b)$$

$$\frac{dw_1'}{dt'} = -v'_{521} + v'_{61} - k_7' w_1' , \quad (1.4a)$$

$$\frac{dw_1'}{dt'} = -k_5' v_1' w_2' + k_6' x_1' - k_7' w_1' , \quad (1.4b)$$

$$\frac{\mathrm{d}x_1'}{\mathrm{d}t'} = v_{521}' + v_{61}' - k_7' x_1', \quad (1.5a)$$

$$\frac{\mathrm{d}x_1'}{\mathrm{d}t'} = k_5' v_2' w_1' - k_6' x_1' - k_7' x_1', \quad (1.5b)$$

$$\frac{\mathrm{d}y_1'}{\mathrm{d}t'} = v'_{71} - k_7' v_1', \quad (1.6a)$$

$$\frac{\mathrm{d}y_1'}{\mathrm{d}t'} = k_8' x_1' - k_7' y_1', \quad (1.6b)$$

$$\frac{\mathrm{d}z_1'}{\mathrm{d}t'} = \beta' + v_{81}' - k_7' z_1', \quad (1.7a)$$

$$\frac{\mathrm{d}z_1'}{\mathrm{d}t'} = \beta' + \theta' \frac{y_1'^2}{y_1'^2 + k_9'^2} - k_7' z_1', \quad (1.7b)$$

$$\frac{dC_2'}{dt'} = q_{rel}{}'_2 - q_{out}{}'_2 - q_{HE}{}'_2 + J'_{WSS}, \quad (1.8a)$$

$$\frac{dC_2'}{dt'} = k_1' \mu' n_2' \left(\frac{b' + C_2'}{1 + C_2'} \right) - k_2' \cdot \frac{C_2'}{k_3' + C_2'} - \zeta' z_2' C_2' + \frac{q'_{max2}}{1 + \alpha \exp\left(-\frac{f_e W(\tau)}{k T_e N} \right)}, \quad (1.8b)$$

$$\frac{\mathrm{d}n_2'}{\mathrm{d}t'} = 1 - n'_{C2} - n_2', \quad (1.9a)$$

$$\frac{\mathrm{d}n_2'}{\mathrm{d}t'} = 1 - \frac{C_2'^2}{1 + C_2'^2} - n_2', \quad (1.9b)$$

$$\frac{\mathrm{d}v_2'}{\mathrm{d}t'} = \beta' + v_{42}' - v_{521}' + v_{61}' - k_7' v_2', \quad (1.10a)$$

$$\frac{\mathrm{d}v_2'}{\mathrm{d}t'} = \beta' + \Theta' \cdot \frac{C_2'^2}{k_4'^2 + C_2'^2} - k_5' v_2' w_1' + k_6' x_2' - k_7' v_2', \quad (1.10b)$$

$$\frac{\mathrm{d}w_2'}{\mathrm{d}t'} = -v_{512}' + v_{62}' - k_7' w_2', \quad (1.11a)$$

$$\frac{\mathrm{d}w_2'}{\mathrm{d}t'} = -k_5' v_2' w_1' + k_6' x_2' - k_7' w_2', \quad (1.11b)$$

$$\frac{\mathrm{d}x_2'}{\mathrm{d}t'} = v_{512}' - v_{62}' - k_7' x_2', \quad (1.12a)$$

$$\frac{\mathrm{d}x_2'}{\mathrm{d}t'} = k_5' v_1' w_2' - k_6' x_2' - k_7' x_2', \quad (1.12b)$$

$$\frac{\mathrm{d}y_2'}{\mathrm{d}t'} = v_{72}' - k_7' v_2', \quad (1.13a)$$

$$\frac{\mathrm{d}y_2'}{\mathrm{d}t'} = k_8' x_2' - k_7' y_2', \quad (1.13b)$$

$$\frac{\mathrm{d}z_2'}{\mathrm{d}t'} = \beta' + v_{82}' - k_7' z_2', \quad (1.14a)$$

$$\frac{\mathrm{d}z_2'}{\mathrm{d}t'} = \beta' + \theta' \frac{y_2'^2}{y_2'^2 + k_9'^2} - k_7' z_2'. \quad (1.14b)$$

Formulas (1.1a)−(1.14b) specify 14 equations for two cells. The indices $i = 1, j = 2$ for the first 7 equations and the indices $i = 2, j = 1$ for the next 7 equations represent numbers of the flows (Table 2) and dynamic variables (Table 1), which refer to the first and second cell respectively (see the left and right cells in Fig. 1). Expressions for flows are given in Table 2, values of dimensionless constants of the model are given in Table 3).

The following initial conditions are used in the model [23] (the index $i = 1, 2$ is the cell number):

$$C'(0)_i = 0.200165,$$

$$n'(0)_i = 0.961477,$$

$$v'(0)_i = 0.1,$$

$$w'(0)_i = 0,$$

$$x'(0)_i = 0,$$

$$y'(0)_i = 0,$$

$$z'(0)_i = 0.$$

Consider the dimensionless parameters that determine the behavior of the system in the magnetic field [19]. The first parameter $m_1 = \frac{P_{magn}}{P_s}$ [19], where P_{mag} is the amplitude of the magnetic wall shear stress, $P_s = 5$ Pa is the WSS corresponding to the saturation of the current through the mechanosensitive Ca^{2+} ion channel, assuming the probability of the opening of channel $f_o = 0.9$ in the Planck model. The parameter m_1 is used for both cases: for the WSS induced by a gradient magnetic field and for the WSS induced by a uniform magnetic field.

The second parameter is $m_2 = \frac{P_s}{\tau_h}$ [19], where τ_h is the WSS due to the blood flow in the vessel, for example, $\tau_h = 1$ Pa for an artery and $\tau_h = 0.1$ Pa for a capillary. The second parameter m_2 does not

depend on magnetic field and therefore serves as a material parameter [19]. We estimate this ratio as $m_2 \approx 5$ for an artery and $m_2 \approx 50$ for a capillary. Thus, the dynamics of calcium concentration is significantly different for an artery and a capillary both for the parameters of the oscillatory mode and for the parameters of the non-oscillatory mode.

The next important parameter that describes the effect of magnetic field on calcium dynamics is the frequency of magnetic field oscillations ν. Thus, we display our further results regarding Ca^{2+} dynamics in coordinates (m_1, ν) for different values m_2 of the parameter associated with different endothelial cells.

A uniform rotating magnetic field with frequencies in the range of 0.01−1 Hz) is effective for controlling the amplitude and frequency of oscillations in the intracellular calcium concentration in endothelial cells [19], as well as in selecting their phenotype. For the same purpose, an inhomogeneous oscillating magnetic field in the same frequency range can be applied (Figs. 4−9).

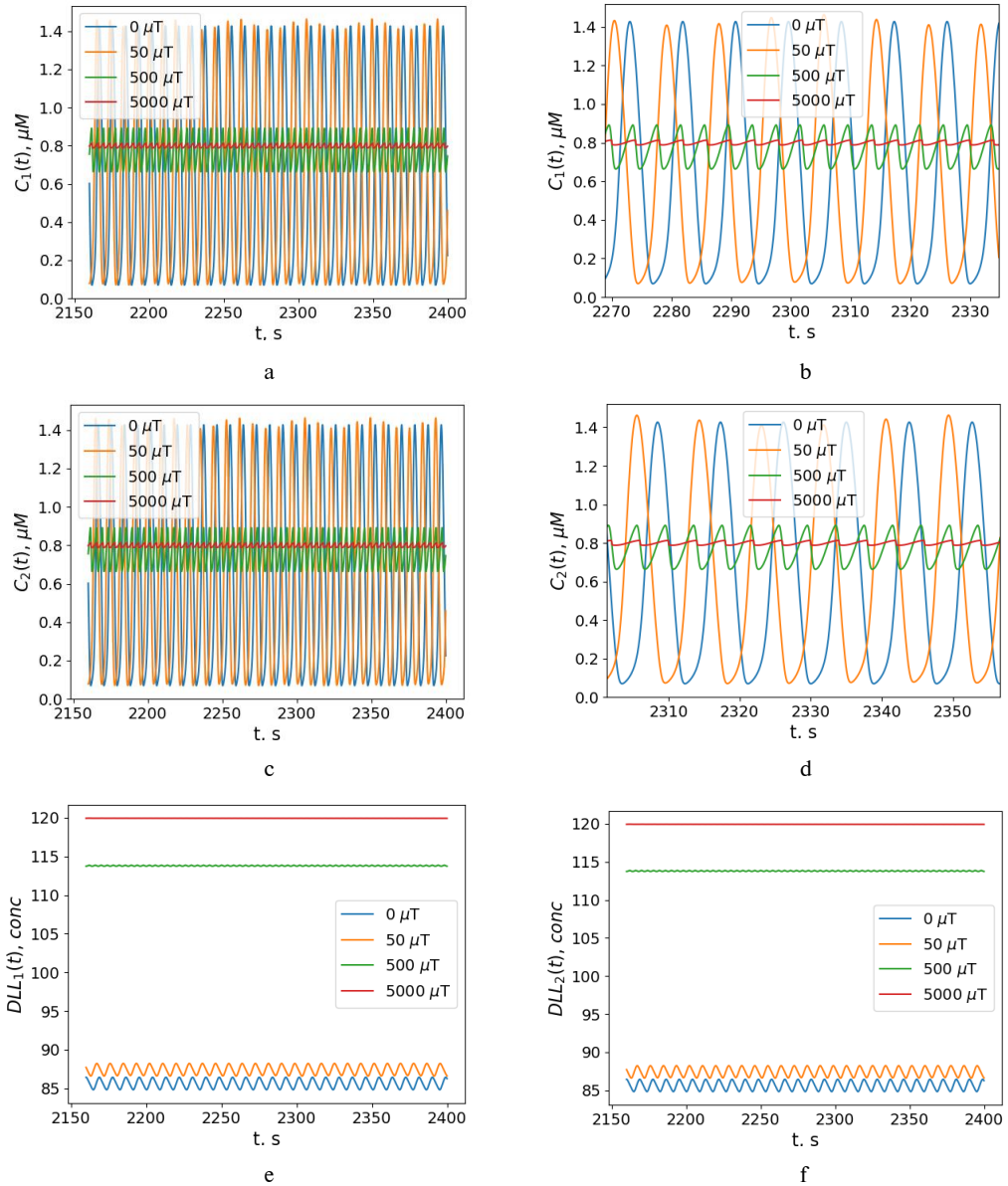

Figure 4: Dynamics of intracellular calcium concentration in the (a, b) first and (c, d) second cells; dynamics of the delta-like ligand (DLL) concentration in the (e) first and (f) second cells for the case of magnetic nanoparticles chains embedded in the membranes of both cells under a rotating magnetic field (from 0 to 5000 μT) with frequency close to the self-oscillation frequency of 1/8 Hz

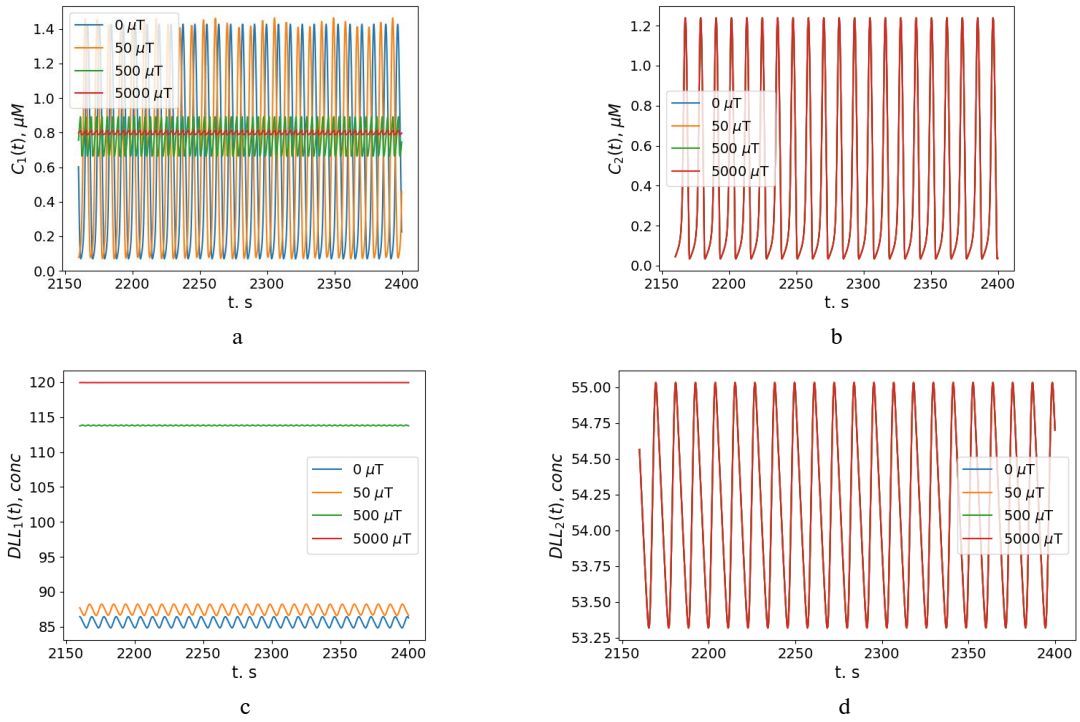

Figure 5: Dynamics of intracellular calcium concentration in the (a) first and (b) second cells; dynamics of the delta-like ligand (DLL) concentration in the (c) first and (d) second cells for the case of magnetic nanoparticles chains embedded in the membrane of only the first cell in a rotating magnetic field (from 0 to 5000 μT) with frequency close to the self-oscillation frequency of 1/8 Hz

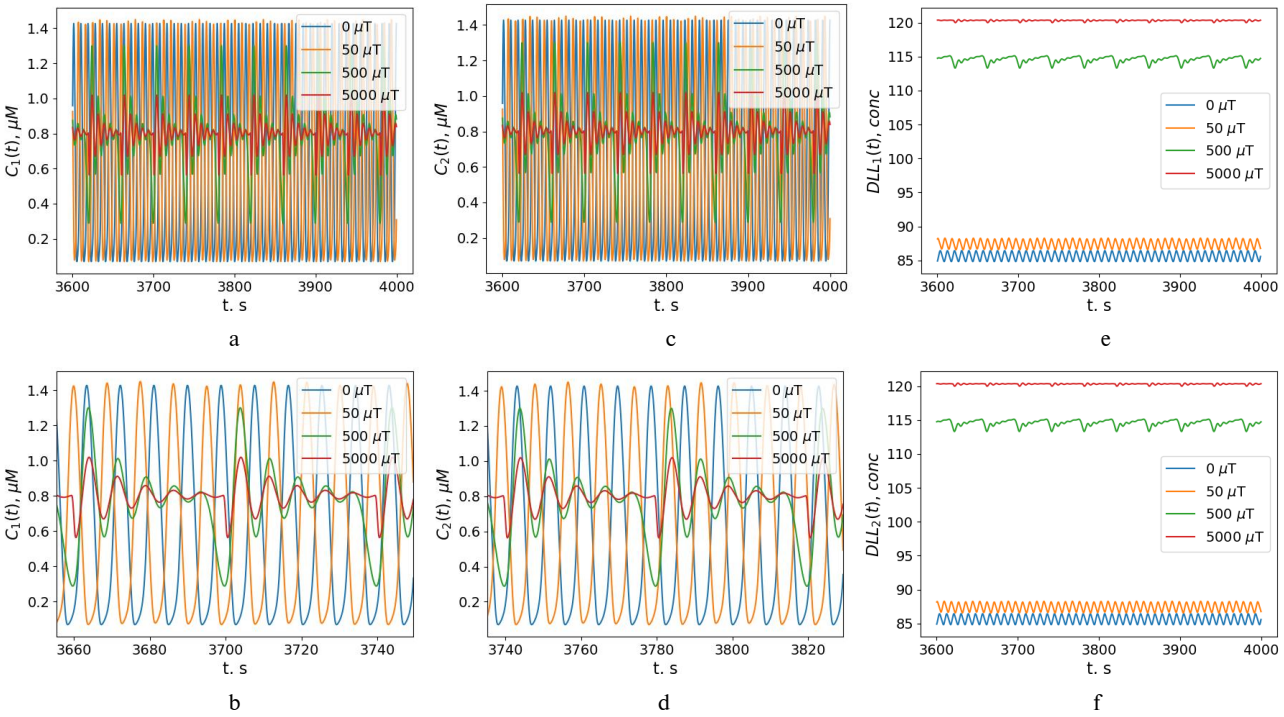

Figure 6: Dynamics of intracellular calcium concentration in the (a, b) first and (c, d) second cells; dynamics of the delta-like ligand (DLL) concentration in the (e) first and (f) second cells for the case of magnetic nanoparticles chains embedded in the membranes of both cells in a rotating magnetic field (from 0 to 5000 μT) with frequency of 1/80 Hz, much lower than the frequency of self-oscillations

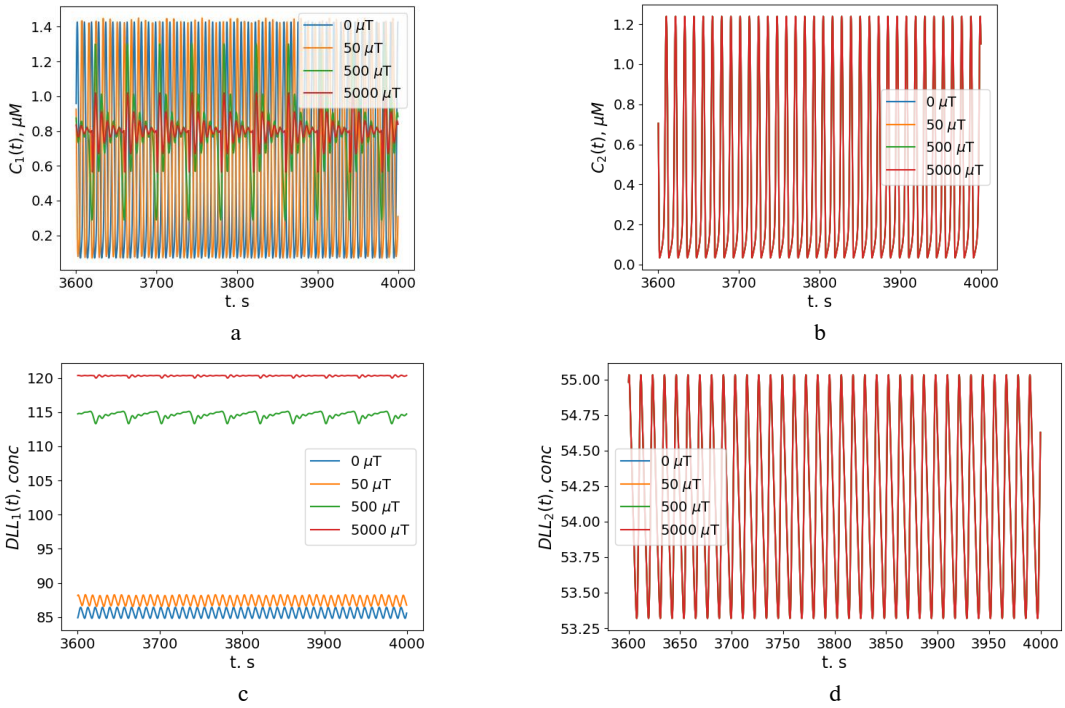

Figure 7: Dynamics of intracellular calcium concentration in the (a) first and (b) second cells; dynamics of the delta-like ligand (DLL) concentration in the (c) first and (d) second cells for the case of magnetic nanoparticles chains embedded in the membrane of only the first cell in a rotating magnetic field (from 0 to 5000 μT) with frequency of 1/80 Hz, which is much lower than the frequency of self-oscillations

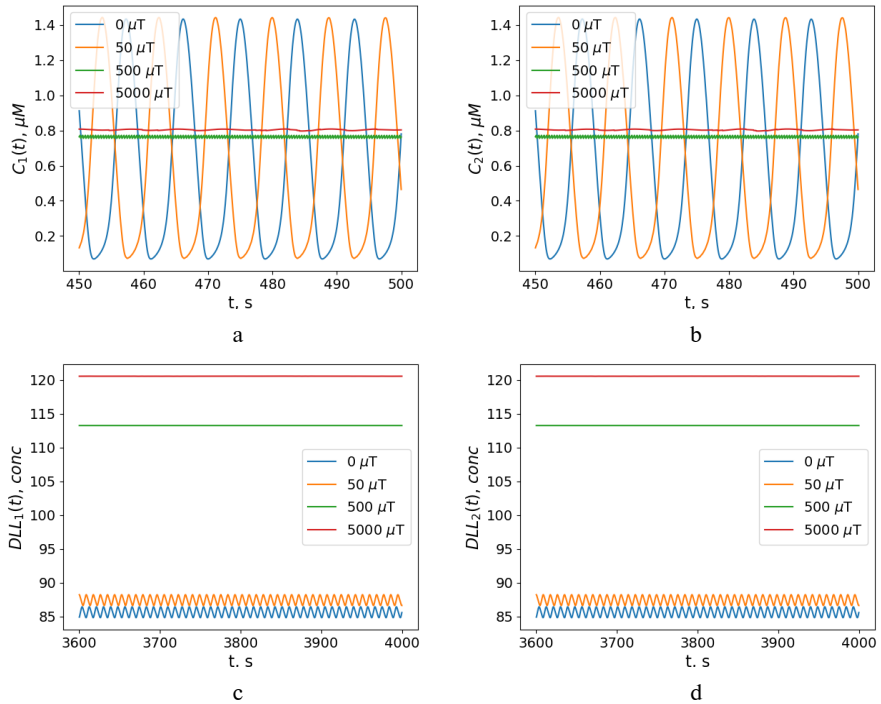

Figure 8: Dynamics of intracellular calcium concentration in the (a) first and (b) second cells; dynamics of the delta-like ligand (DLL) concentration in the (c) first and (d) second cells for the case of magnetic nanoparticles chains embedded in the membranes of both cells in a rotating magnetic field (from 0 to 5000 μT) with frequency of 10/8 Hz, much higher than the frequency of self-oscillations

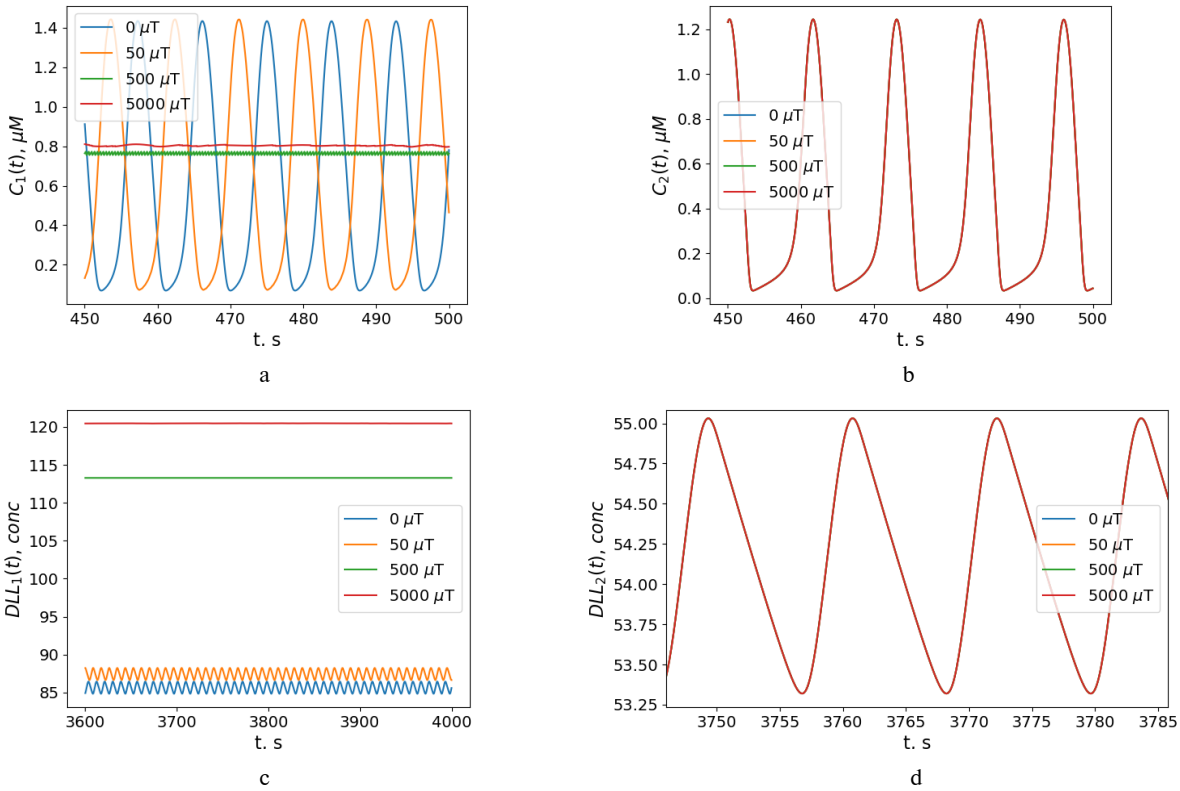

Figure 9: Dynamics of intracellular calcium concentration in the (a) first and (b) second cells; dynamics of the delta-like ligand (DLL) concentration in the (c) first and (d) second cells for the case of magnetic nanoparticles chains embedded in the membrane of only the first cell in a rotating magnetic field (from 0 to 5000 μT) with frequency of 10/8 Hz, which is much higher than the frequency of self-oscillations

The natural frequency of calcium oscillations is in the range from tens of millihertz to tens of hertz as it is observed experimentally [41]. To achieve the effect of the magnetic field to be resonant, it is reasonable to choose magnetic field frequencies that are close to the frequency of self-oscillations of concentration of intracellular calcium. Higher and lower frequencies have less effect, because they lie far from the frequency of self-oscillations, i.e. from the resonant frequency (Figs. 4–9). In low magnetic fields with frequencies that coincide with the frequencies of self-oscillations of calcium concentration in endothelial cells it is possible to achieve a significant effect on endothelial cell phenotype due to its resonant nature. One more advantage of sufficiently low frequencies is that the magnetic field does not cause thermal effects on magnetic nanoparticles at such frequencies unlike the technique of magnetic hyperthermia. Besides, the choice of low frequency magnetic field application will simplify the design of the magnetic device and expand the range of magnetic field inductions.

Discussion

The concentration of DLL changes by 1.3–1.4 times under a uniform rotating external low-frequency magnetic field in the presence of MNPs embedded in the cell membrane. It allows controlling the phenotype of endothelial cells. Indeed, as can be seen from Figs. 4–9, a magnetic field can suppress oscillations of the intracellular calcium concentration changing the cell phenotype from tip cells to stalk cells (following), because according to the conclusions of works [23, 42] these oscillations are preserved only in cells, that choose the tip cell phenotype. Also, the magnetic field (see Fig. 4–9) can significantly increase the concentration of DLL4, which is also decisive for the selection of tip phenotype by cells, because a cell with significantly higher levels of DLL4 is defined as a tip cell according to experimental and theoretical works [23, 42]. At the same time, the attachment of MNPs to the membrane of only one of the two neighboring cells allows the magnetic field to target only its pheno-

type without changing the phenotype of the neighboring cell. Such targeting of the gating of calcium ion channels to specific cells is promising because other methods of targeting at ion channels (using low molecular weight compounds, monoclonal antibodies) are not cell-specific and are not selective even for one therapeutic area.

Tissue branching morphogenesis necessitates the hierarchical arrangement of sprouting endothelial cells into leading "tip" cells and trailing "stalk" cells [43]. During angiogenesis, endothelial tip cells guide the sprouting vessels, extend filopodia, and migrate in response to gradients of vascular endothelial growth factor. In contrast, stalk cells follow the tip cells, forming the trunk of new vessels and maintaining connectivity with the parent vessels [44]. The processes of tip-stalk endothelial cell phenotype selection form the foundation of sprouting angiogenesis. Going forward, regulators of these processes may serve as potential markers and targets for angiogenesis [45]. Endothelial cell diversity is crucial for the formation, maintenance, and regeneration of the vascular system during development and disease, particularly in wound healing [46]. The plasticity of endothelial cells have significant implications for disease progression, especially in scarring and fibrosis [46]. Choice of endothelial cell phenotype is crucial for insights into vasculargenesis and angiogenesis in diseases like cancer [46]. Therapeutic modulation of vascular cell proliferation and migration is essential for the effective inhibition of angiogenesis in cancer or its induction in cardiovascular disease [47]. That is why the results of the present research open the new non-invasive way of magnetic control of angiogenesis for treatment of cancer, cardiovascular diseases and wound healing.

The experimental verification of the results of the manuscript is possible because:

– there are technologies of production and administration of artificial magnetic nanoparticles in target organ, see for example, [48–51];

– magnetic systems for creation of low frequency weak and moderate magnetic fields are wide spread and not expensive, see for example, [52, 53];

– the methods of phenotyping of endothelial cells are developed, see for example, [54, 55];

– the methods of *in vivo* measurements of calcium oscillations in endothelial cells are developed, see for example, [42, 56].

The experimental verification of the results of the present modelling is perspective in both cases, i.e. with or without administration of artificial magnetic nanoparticles because there are biogenic magnetic nanoparticles in human organs and tissues. For example, the review papers describe in detail the localization in tissues and organs, concentration, morphology and physical properties of biogenic magnetic nanoparticles [17, 18, 57].

In view of the above considerations, there [48] are some experimental studies dedicated to the influence of magnetic fields on biological samples containing magnetic nanoparticles [58], and electromagnetic fields without the use of magnetic nanoparticles [59], on growth factors, leading to the conclusion that effects are present and controlled influence is possible. Other experiments are also reported involving changes in the phenotype or morphology of organic structures, such as macrophages [60] and osteoblasts [61], under the influence of a magnetic field.

Conclusions

The choice of phenotype by endothelial cells can be controlled in a uniform rotating external low-frequency magnetic field, as well as in a gradient oscillating magnetic field, which opens the way to control angiogenesis and vascular architecture.

The novelty of the paper lies in presenting, for the first time, the results of theoretical modeling of the low frequency moderate magnetic field's non-thermal influence on magnetic nanoparticles embedded in the membranes of endothelial cells for controlling the phenotype of endothelial cells.

List of abbreviations

WSS – wall shear stress

MF – magnetic field

DLL4 – delta-like 4 protein, a transmembrane protein that activates the Notch pathway

IP3 – inositol 1,4,5-trisphosphate

IP3R – IP3 receptor

ECs – endothelial cells

VEGF – vascular endothelial growth factor

HE – hairy and enhancer-of-split family of proteins

SERCA – sarco/endoplasmic reticulum Ca^{2+}-ATPase

ER – endoplasmic reticulum

CICR – calcium induced-calcium release

Notch – a family of type-1 transmembrane proteins that form a core component of the Notch signaling pathway, which is highly conserved in metazoans

NICD – Notch intracellular domain

BMN – biogenic magnetic nanoparticles
SD – single domain
MNP – magnetic nanoparticles
RMF – rotating magnetic field

Interests disclosure

The authors of the article confirm the absence of a conflict of interest.

References

[1] Dorofteiu M, Morariu VV, Marina C, Zirbo M. The effects of near null magnetic field upon the leucocyte response in rats. Cytobios. 1995;84(338-339):179-89.

[2] Tao R, Huang K. Reducing blood viscosity with magnetic fields. Phys Rev E Stat Nonlin Soft Matter Phys. 2011;84(1 Pt 1):011905. DOI: 10.1103/PhysRevE.84.011905

[3] Yamamoto T, Nagayama Y, Tamura M. A blood-oxygenation-dependent increase in blood viscosity due to a static magnetic field. Phys Med Biol. 2004 Jul 21;49(14):3267-77. DOI: 10.1088/0031-9155/49/14/017

[4] Trofimov AV, Sevostyanova EV. Dynamics of blood values in experimental geomagnetic deprivation (in vitro) reflects biotropic effects of natural physical factors during early human ontogeny. Bull Exp Biol Med. 2008 Jul;146(1):100-3. DOI: 10.1007/s10517-008-0221-4

[5] Ciorba D, Morariu VV. Life in zero magnetic field. iii. activity of aspartate aminotransferase and alanine aminotransferase during in vitro aging of human blood. Electro Magnetobiol. 2001;20:313-21. DOI: 10.1081/JBC-100108572

[6] Martino CF, Perea H, Hopfner U, Ferguson VL, Wintermantel E. Effects of weak static magnetic fields on endothelial cells. Bioelectromagnetics. 2010 May;31(4):296-301. DOI: 10.1002/bem.20565

[7] Martino CF. Static magnetic field sensitivity of endothelial cells. Bioelectromagnetics. 2011;32(6):506-8. DOI: 10.1002/bem.20665

[8] McKay JC, Prato FS, Thomas AW. A literature review: the effects of magnetic field exposure on blood flow and blood vessels in the microvasculature. Bioelectromagnetics. 2007 Feb;28(2):81-98. DOI: 10.1002/bem.20284

[9] Weber RV, Navarro A, Wu JK, Yu HL, Strauch B. Pulsed magnetic fields applied to a transferred arterial loop support the rat groin composite flap. Plast Reconstr Surg. 2004 Oct;114(5):1185-9. DOI: 10.1097/01.prs.0000135857.95310.13

[10] Tepper OM, Callaghan MJ, Chang EI, Galiano RD, Bhatt KA, Baharestani S, et al. Electromagnetic fields increase in vitro and in vivo angiogenesis through endothelial release of FGF-2. FASEB J. 2004;18(11):1231-3. DOI: 10.1096/fj.03-0847fje

[11] Greenough CG. The effects of pulsed electromagnetic fields on blood vessel growth in the rabbit ear chamber. J Orthop Res. 1992 Mar;10(2):256-62. DOI: 10.1002/jor.1100100213

[12] Roland D, Ferder M, Kothuru R, Faierman T, Strauch B. Effects of pulsed magnetic energy on a microsurgically transferred vessel. Plast Reconstr Surg. 2000 Apr;105(4):1371-4. DOI: 10.1097/00006534-200004040-00016

[13] Yen-Patton GP, Patton WF, Beer DM, Jacobson BS. Endothelial cell response to pulsed electromagnetic fields: stimulation of growth rate and angiogenesis in vitro. J Cell Physiol. 1988 Jan;134(1):37-46. DOI: 10.1002/jcp.1041340105

[14] Ottani V, De Pasquale V, Govoni P, Franchi M, Zaniol P, Ruggeri A. Effects of pulsed extremely-low-frequency magnetic fields on skin wounds in the rat. Bioelectromagnetics. 1988;9(1):53-62. DOI: 10.1002/bem.2250090105

[15] Williams CD, Markov MS, Hardman WE, Cameron IL. Therapeutic electromagnetic field effects on angiogenesis and tumor growth. Anticancer Res. 2001 Nov-Dec;21(6A):3887-91.

[16] Ruggiero M, Bottaro DP, Liguri G, Gulisano M, Peruzzi B, Pacini S. 0.2 T magnetic field inhibits angiogenesis in chick embryo chorioallantoic membrane. Bioelectromagnetics. 2004 Jul;25(5):390-6. DOI: 10.1002/bem.20008

[17] Gorobets S, Gorobets O, Gorobets Y, Bulaievska M. Chain-Like Structures of Biogenic and Nonbiogenic Magnetic Nanoparticles in Vascular Tissues. Bioelectromagnetics. 2022 Feb;43(2):119-43. DOI: 10.1002/bem.22390

[18] Gorobets O, Gorobets S, Sharai I, Polyakova T, Zablotskii V. Interaction of magnetic fields with biogenic magnetic nanoparticles on cell membranes: Physiological consequences for organisms in health and disease. Bioelectrochemistry. 2023 Jun;151:108390. DOI: 10.1016/j.bioelechem.2023.108390

[19] Gorobets O, Gorobets S, Polyakova T, Zablotskii V. Modulation of calcium signaling and metabolic pathways in endothelial cells with magnetic fields. Nanoscale Adv. 2024 Jan 23;6(4):1163-82. DOI: 10.1039/d3na01065a

[20] Hughes S, McBain S, Dobson J, El Haj AJ. Selective activation of mechanosensitive ion channels using magnetic particles. J R Soc Interface. 2008 Aug 6;5(25):855-63. DOI: 10.1098/rsif.2007.1274

[21] Unnithan AR, Rotherham M, Markides H, El Haj AJ. Magnetic ion channel activation (MICA)-enabled screening assay: A dynamic platform for remote activation of mechanosensitive ion channels. Int J Mol Sci. 2023 Feb 8;24(4):3364. DOI: 10.3390/ijms24043364

[22] Hao L, Li L, Wang P, Wang Z, Shi X, Guo M, Zhang P. Synergistic osteogenesis promoted by magnetically actuated nano-mechanical stimuli. Nanoscale. 2019 Dec 28;11(48):23423-37. DOI: 10.1039/c9nr07170a

[23] Debir B, Meaney C, Kohandel M, Unlu MB. The role of calcium oscillations in the phenotype selection in endothelial cells. Sci Rep. 2021 Dec 10;11(1):23781. DOI: 10.1038/s41598-021-02720-2

[24] Plank MJ, Wall DJ, David T. Atherosclerosis and calcium signalling in endothelial cells. Prog Biophys Mol Biol. 2006 Jul;91(3):287-313. DOI: 10.1016/j.pbiomolbio.2005.07.005

[25] Kostyuk PG. Diversity of calcium ion channels in cellular membranes. Neuroscience. 1989;28(2):253-61. DOI: 10.1016/0306-4522(89)90177-2

[26] Heine M, Heck J, Ciuraszkiewicz A, Bikbaev A. Dynamic compartmentalization of calcium channel signalling in neurons. Neuropharmacology. 2020 Jun 1;169:107556. DOI: 10.1016/j.neuropharm.2019.02.038

[27] Findlay I, Suzuki S, Murakami S, Kurachi Y. Physiological modulation of voltage-dependent inactivation in the cardiac muscle L-type calcium channel: a modelling study. Prog Biophys Mol Biol. 2008;96(1-3):482-98. DOI: 10.1016/j.pbiomolbio.2007.07.002

[28] Alexander S, Mathie A, Peters J. Ion channels. Br J Pharmacol 2011;164:S137-74. DOI: 10.1111/j.1476-5381.2011.01649_5.x

[29] Peyronnet R, Tran D, Girault T, Frachisse JM. Mechanosensitive channels: feeling tension in a world under pressure. Front Plant Sci. 2014 Oct 21;5:558. DOI: 10.3389/fpls.2014.00558

[30] Catterall WA, Perez-Reyes E, Snutch TP, Striessnig J. International Union of Pharmacology. XLVIII. Nomenclature and structure-function relationships of voltage-gated calcium channels. Pharmacol Rev. 2005;57(4):411-25. DOI: 10.1124/pr.57.4.5

[31] Dash S, Das T, Patel P, Panda PK, Suar M, Verma SK. Emerging trends in the nanomedicine applications of functionalized magnetic nanoparticles as novel therapies for acute and chronic diseases. J Nanobiotechnology. 2022 Aug 31;20(1):393. DOI: 10.1186/s12951-022-01595-3

[32] Bridge G, Monteiro R, Henderson S, Emuss V, Lagos D, Georgopoulou D, et al. The microRNA-30 family targets DLL4 to modulate endothelial cell behavior during angiogenesis. Blood. 2012;120(25):5063-72. DOI: 10.1182/blood-2012-04-423004

[33] Leach A, Smyth P, Ferguson L, Steven J, Greene MK, Branco CM, et al. Anti-DLL4 VNAR targeted nanoparticles for targeting of both tumour and tumour associated vasculature. Nanoscale. 2020;12(27):14751-63. DOI: 10.1039/d0nr02962a

[34] Trindade A, Djokovic D, Gigante J, Mendonɜa L, Duarte A. Endothelial Dll4 overexpression reduces vascular response and inhibits tumor growth and metastasization in vivo. BMC Cancer. 2017 Mar 14;17(1):189. DOI: 10.1186/s12885-017-3171-2

[35] Lobov IB, Renard RA, Papadopoulos N, Gale NW, Thurston G, Yancopoulos GD, et al. Delta-like ligand 4 (Dll4) is induced by VEGF as a negative regulator of angiogenic sprouting. Proc Natl Acad Sci U S A. 2007 Feb 27;104(9):3219-24. DOI: 10.1073/pnas.0611206104

[36] Atri A, Amundson J, Clapham D, Sneyd J. A single-pool model for intracellular calcium oscillations and waves in the Xenopus laevis oocyte. Biophys J. 1993 Oct;65(4):1727-39. DOI: 10.1016/S0006-3495(93)81191-3

[37] Venkatraman L, Regan ER, Bentley K. Time to Decide? Dynamical Analysis Predicts Partial Tip/Stalk Patterning States Arise during Angiogenesis. PLoS One. 2016 Nov 15;11(11):e0166489. DOI: 10.1371/journal.pone.0166489

[38] Skalak R, Tozeren A, Zarda RP, Chien S. Strain energy function of red blood cell membranes. Biophys J. 1973;13(3):245-64. DOI: 10.1016/S0006-3495(73)85983-1

[39] Wiesner TF, Berk BC, Nerem RM. A mathematical model of the cytosolic-free calcium response in endothelial cells to fluid shear stress. Proc Natl Acad Sci U S A. 1997 Apr 15;94(8):3726-31. DOI: 10.1073/pnas.94.8.3726

[40] Roux E, Bougaran P, Dufourcq P, Couffinhal T. Fluid Shear Stress Sensing by the Endothelial Layer. Front Physiol. 2020 Jul 24;11:861. DOI: 10.3389/fphys.2020.00861

[41] Smedler E, Uhlén P. Frequency decoding of calcium oscillations. Biochim Biophys Acta. 2014 Mar;1840(3):964-9. DOI: 10.1016/j.bbagen.2013.11.015

[42] Yokota Y, Nakajima H, Wakayama Y, Muto A, Kawakami K, Fukuhara S, et al. Endothelial Ca^{2+} oscillations reflect VEGFR signaling-regulated angiogenic capacity in vivo. Elife. 2015;4. DOI: 10.7554/eLife.08817

[43] Malek AM, Izumo S. Control of endothelial cell gene expression by flow. J Biomech. 1995 Dec;28(12):1515-28. DOI: 10.1016/0021-9290(95)00099-2

[44] Herbert SP, Cheung JY, Stainier DY. Determination of endothelial stalk versus tip cell potential during angiogenesis by H2.0-like homeobox-1. Curr Biol. 2012 Oct 9;22(19):1789-94. DOI: 10.1016/j.cub.2012.07.037

[45] Chen W, Xia P, Wang H, Tu J, Liang X, Zhang X, et al. The endothelial tip-stalk cell selection and shuffling during angiogenesis. J Cell Commun Signal. 2019 Sep;13(3):291-301. DOI: 10.1007/s12079-019-00511-z

[46] Gurevich DB, David DT, Sundararaman A, Patel J. Endothelial heterogeneity in development and wound healing. Cells. 2021 Sep 7;10(9):2338. DOI: 10.3390/cells10092338

[47] Mühleder S, Fernández-Chacón M, Garcia-Gonzalez I, Benedito R. Endothelial sprouting, proliferation, or senescence: tipping the balance from physiology to pathology. Cell Mol Life Sci. 2021;78(4):1329-54. DOI: 10.1007/s00018-020-03664-y

[48] Prijic S, Sersa G. Magnetic nanoparticles as targeted delivery systems in oncology. Radiol Oncol. 2011 Mar;45(1):1-16. DOI: 10.2478/v10019-011-0001-z

[49] Alirezaie Alavijeh A, Barati M, Barati M, Abbasi Dehkordi H. The potential of magnetic nanoparticles for diagnosis and treatment of cancer based on body magnetic field and organ-on-the-chip. Adv Pharm Bull. 2019 Aug;9(3):360-73. DOI: 10.15171/apb.2019.043

[50] Mody VV, Cox A, Shah S, Singh A, Bevins W, Parihar H. Magnetic nanoparticle drug delivery systems for targeting tumor. Appl Nanosci. 2014;4:385-92. DOI: 10.1007/s13204-013-0216-y

[51] Chenthamara D, Subramaniam S, Ramakrishnan SG, Krishnaswamy S, Essa MM, Lin FH, et al. Therapeutic efficacy of nanoparticles and routes of administration. Biomater Res. 2019 Nov 21;23:20. DOI: 10.1186/s40824-019-0166-x

[52] Judakova Z, Janousek L, Radil R, Carnecka L. Low-frequency magnetic field exposure system for cells electromagnetic biocompatibility studies. Appl Sci. 2022;12:6846. DOI: 10.3390/app12146846

[53] Li Y, Chen Z, Liu Y, Liu Z, Wu T, Zhang Y, et al. Ultra-low frequency magnetic energy focusing for highly effective wireless powering of deep-tissue implantable electronic devices. Natl Sci Rev. 2024;11(5):nwae062. DOI: 10.1093/nsr/nwae062

[54] Grant D, Wanner N, Frimel M, Erzurum S, Asosingh K. Comprehensive phenotyping of endothelial cells using flow cytometry 2: Human. Cytometry A. 2021 Mar;99(3):257-64. DOI: 10.1002/cyto.a.24293

[55] Blanco R, Gerhardt H. VEGF and Notch in tip and stalk cell selection. Cold Spring Harb Perspect Med. 2013;3(1):a006569. DOI: 10.1101/cshperspect.a006569

[56] Moccia F, Brunetti V, Soda T, Berra-Romani R, Scarpellino G. Cracking the endothelial calcium (Ca^{2+}) code: A matter of timing and spacing. Int J Mol Sci. 2023 Nov 26;24(23):16765. DOI: 10.3390/ijms242316765

[57] Gorobets O, Gorobets S, Koralewski M. Physiological origin of biogenic magnetic nanoparticles in health and disease: from bacteria to humans. Int J Nanomedicine. 2017 Jun 12;12:4371-95. DOI: 10.2147/IJN.S130565

[58] Manjua AC, Cabral JMS, Portugal CAM, Ferreira FC. Magnetic stimulation of the angiogenic potential of mesenchymal stromal cells in vascular tissue engineering. Sci Technol Adv Mater. 2021;22(1):461-80. DOI: 10.1080/14686996.2021.1927834

[59] Chen J, Tu C, Tang X, Li H, Yan J, Ma Y, et al. The combinatory effect of sinusoidal electromagnetic field and VEGF promotes osteogenesis and angiogenesis of mesenchymal stem cell-laden PCL/HA implants in a rat subcritical cranial defect. Stem Cell Res Ther. 2019 Dec 16;10(1):379. DOI: 10.1186/s13287-019-1464-x

[60] Wosik J, Chen W, Qin K, Ghobrial RM, Kubiak JZ, Kloc M. Magnetic field changes macrophage phenotype. Biophys J. 2018 Apr 24;114(8):2001-13. DOI: 10.1016/j.bpj.2018.03.002

[61] Qian AR, Gao X, Zhang W, Li JB, Wang Y, Di SM, et al. Large gradient high magnetic fields affect osteoblast ultrastructure and function by disrupting collagen I or fibronectin/αβ1 integrin. PLoS One. 2013;8(1):e51036. DOI: 10.1371/journal.pone.0051036

С.В. Горобець, О.Ю. Горобець* , К.О. Рачек, А.М. Рязанова

КПІ ім. Ігоря Сікорського, Київ, Україна

ВПЛИВ МАГНІТНОГО ПОЛЯ ТА МАГНІТНИХ НАНОЧАСТИНОК НА ВИБІР ФЕНОТИПУ ЕНДОТЕЛІАЛЬНИХ КЛІТИН

Проблематика. Ендотеліальні клітини як учасники ангіогенезу вибирають свій фенотип як кінчикові клітини (провідні, мігруючі) або клітини стебла (наступні). Експериментально виявлено та теоретично змодельовано, що швидкі коливання концентрації кальцію всередині клітини відіграють ключову роль у контролі вибору фенотипу та можливої архітектури судин. Крім того, відомо, що внутрішньоклітинна концентрація кальцію в ендотеліальних клітинах регулюється механічним напруження зсуву мембрани, спричиненим кровотоком, який контролює механочутливі канали іонів кальцію. Розроблено експериментальні методи керування механочутливими іонними каналами в зовнішніх магнітних полях із застосуванням магнітних наночастинок, що впливають на магнітні наночастинки, штучно прикріплені до клітинних мембран.

Мета. Порушується ключове питання щодо можливості контрольованого вибору фенотипу ендотеліальних клітин у зовнішніх магнітних полях за рахунок наявності штучних або біогенних магнітних наночастинок, вбудованих у клітинну мембрану.

Методика реалізації. Розраховано магнітне напруження зсуву мембрани внаслідок впливу зовнішнього магнітного поля на магнітні наночастинки, вбудовані в мембрану клітини, яке контролює механочутливі іонні канали кальцію. Здійснено числове моделювання коливань внутрішньоклітинної концентрації кальцію в ендотеліальних клітинах та визначення їхнього кінцевого фенотипу з урахуванням міжклітинної комунікації. Для числового моделювання використано мову програмування python та пакети scipy, py-pde, matplotlib мови програмування python.

Результати. Розраховано діапазони індукції та частоти однорідного обертового магнітного поля, а також величину градієнта і частоту неоднорідного осцилюючого магнітного поля для управління амплітудою та частотою коливань внутрішньоклітинної концентрації кальцію в ендотеліальних клітинах, а також вибором їх фенотипу.

Висновки. Вибір фенотипу ендотеліальними клітинами може бути керований в однорідному обертовому зовнішньому магнітному полі, а також в неоднорідному осцилюючому магнітному полі, що відкриває шлях до керування ангіогенезом і архітектурою судин.

Ключові слова: градієнт магнітного поля; обертове магнітне поле; ендотеліальні клітини; внутрішньоклітинна концентрація кальцію; вибір фенотипу; магнітні наночастинки.